THE JOURNAL OF PHYSICAL CHEMISTRY A
A JOURNAL OF THE AMERICAN CHEMICAL SOCIETY

pubs.acs.org/JPCA

Article

Dynamics of Transition Metal Ion Transport in High-Gradient Magnetic Fields

Prateek Benhal, Muhammad Garba, Jamel Ali, Theo Siegrist, Munir Humayun, and Hadi Mohammadigoushki*

Cite This: *J. Phys. Chem. A* 2025, 129, 3401−3410

Read Online

ACCESS | Metrics & More | Article Recommendations | Supporting Information

ABSTRACT: Magnetic separation has emerged as an eco-friendly and sustainable technique with applications in water purification, chemical separation, biochemistry, medicine, and mining. In this study, we present a combined experimental and theoretical investigation of the transport of transition metal ions using high-gradient magnetic fields. Experiments were conducted on aqueous solutions containing either paramagnetic manganese chloride ($MnCl_2$) or diamagnetic zinc chloride ($ZnCl_2$) ions, with concentrations ranging from 1 to 100 mM under a non-uniform magnetic field of an electromagnet. Our results demonstrate that while paramagnetic $MnCl_2$ is captured by the mesh wool in the magnetic field, diamagnetic $ZnCl_2$ remains unaffected by the presence of a magnetic field. The capture efficiency of paramagnetic $MnCl_2$ increases with both the initial ion concentration and the applied magnetic field strength. Furthermore, in binary mixtures, the capture rate of $MnCl_2$ is reduced compared with single-ion solutions, highlighting the role of ion interactions in magnetic separation. Our theoretical modeling indicates that magnetic capture is governed by a balance between magnetic forces and viscous forces. Additionally, the magnetic separation process is enhanced by the field-induced cluster formation of paramagnetic metal ions, which are predicted to be 2 orders of magnitude larger than individual hydrated ion units. These findings provide insights into the mechanisms of magnetic transport of metal ions and offer potential pathways for improving separation efficiency in complex ion mixtures that contain critical materials.

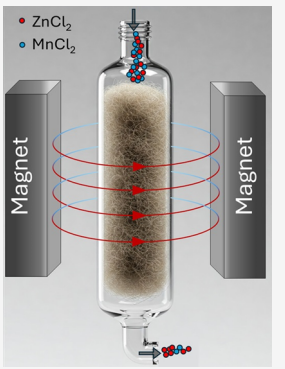

1. INTRODUCTION

Following the discovery of Faraday on electromagnetism, magnetic separation has long been used as a technique to separate components of a mixture based on their magnetic properties.[1] This method has found applications in a wide range of processes, from the nuclear industry, drug delivery,[2] in chemical kinetics,[3] water purification[4,5] as well as in biochemical and medical fields.[6,7] As the global economy shifts toward sustainable and renewable energy sources, lithium-ion batteries (LIBs) are increasingly used in almost every electronic product. With the ever-growing need for LIB production, multimillion tons of LIBs will reach their end of life in the near future and, if not properly recycled, could potentially lead to a detrimental impact on natural resources, supply chain, environment, and energy conservation. LIBs, together with a wide range of electronic equipment, contain critical metals such as lithium, nickel, cobalt, and manganese, and a key challenge in their recycling is the effective separation of these metal ions from mixed solutions. Current separation methods for these metals are costly, energy-intensive, and cause significant environmental pollution.[8−10] Consequently, there is a pressing need for greener and more environmentally friendly separation techniques. The critical metals found in spent lithium-ion batteries (LIBs) and other electronic equipment display a wide range of magnetic susceptibilities, with some being paramagnetic and others being diamagnetic. A paramagnetic material is weakly attracted to a magnetic field, while a diamagnetic material is repelled by a magnetic field. Magnetic separation presents an environmentally sustainable option by reducing waste, improving recycling efficiency, minimizing pollution, and conserving energy.[11−14] These advantages make it a promising alternative for recycling critical metals from end-of-life LIBs and other waste streams.[8]

The conventional magnetic separation devices employ a low gradient magnetic field (LGMS) and are typically limited to separating strongly magnetic materials, such as iron and magnetite, from weakly magnetic materials such as apatite.[15] Recognizing that the primary driving force behind magnetic separation is the magnetic field gradient, high-gradient magnetic field separators were invented.[1,15−18] The main component of high-gradient magnetic field separators involves the presence of a ferromagnetic matrix (in the form of a mesh of wires or grooved plates[19−21]) in a uniform magnetic field. Over the past 50 years, high-gradient magnetic field separation (HGMS) has attracted considerable interest both experimen-

Received: December 9, 2024
Revised: March 26, 2025
Accepted: March 26, 2025
Published: April 9, 2025

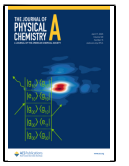

https://doi.org/10.1021/acs.jpca.4c08312
J. Phys. Chem. A 2025, 129, 3401−3410

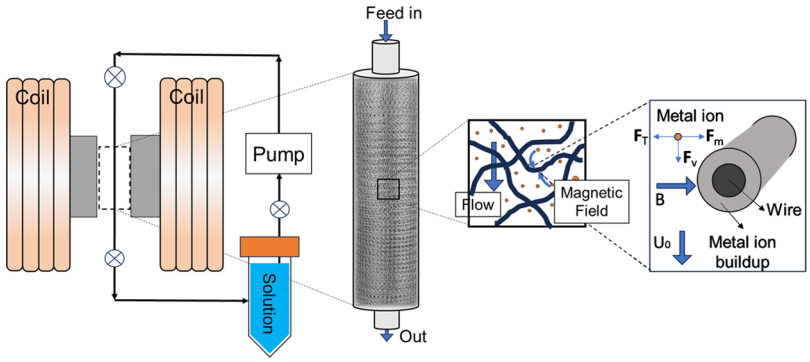

Figure 1. Schematic showing the experimental setup for the separation of metal ions. The separation chamber is placed inside a uniform magnetic field between the pole pieces. Once the flow is initiated, whether in the presence or absence of a magnetic field, we extract 1 mL of solution from the solution reservoir (highlighted in blue) in 1 h time interval and measure its concentration. Here, $\mathbf{F}_T$, $\mathbf{F}_m$, and $\mathbf{F}_v$ refer to thermal diffusion and magnetic and viscous forces, respectively.

tally and theoretically. HGMS has typically been successful in efficiently separating the micrometer-scale particles or larger aggregates.[22−29] There are a few studies that have shown nanoparticles could be captured by the HGMS if they form clusters[30,31] but there is a dearth of HGMS applications to particles from nanometer to atomic scales.

Previous theoretical studies have explored the transport and separation of fine particles in high-gradient magnetic separators (HGMS) through various modeling approaches, including trajectory analysis[32,33] and stochastic[34] or phenomenological models.[35−37] The first attempt to model the HGMS process was made by Watson in 1973.[32] Watson numerically solved the problem of the trajectory of a paramagnetic particle around a ferromagnetic wire by considering inertia and ignoring the effects of viscous and gravitational forces, and developed a relation to assess the change in concentration of fine (typically several micrometer in size) particles as they exit the HGMS filter.[32,33] Motivated by some disagreements between the trajectory model and experiments,[38] other researchers developed a filtration model that takes into account the probability of particle collision and retention on the filter.[34] More recently, other researchers have developed phenomenological models.[35−37] However, these models suffer from several simplifying assumptions. For example, these models are developed for static HGMS and do not account for the time-dependent capture of particles in the system. In addition, these models do not consider the effects of buildup on the filter. As particles move through the mesh, the ability of the mesh to attract more particles decreases. More recently, Hatton and co-workers developed a model for capturing superparamagnetic nanoparticles, employing a simple force balance that accounts for the effects of viscous forces at vanishingly small Reynolds numbers, particle accumulation under flow and diffusion-limited conditions.[30,31]

Despite significant advances in understanding the separation of fine particles (micro- and nanosized) using high-gradient magnetic fields, a substantial gap remains in determining whether this method can effectively separate metal ions, which are considerably smaller than the finest particles to which HGMS has been successfully applied. At the scale of hydrated metal ions (in the order of several Å), in the absence of inertia, diffusive forces become highly significant. Additionally, transition-metal ions, including those found in LIBs, are either paramagnetic or diamagnetic, exhibiting weak magnetizations. Consequently, due to the small size of the ions and their weak magnetic properties, the magnetic force driving their capture by the magnetic mesh is expected to be much weaker than the thermal diffusive forces resisting this capture (see details of analysis in pp 6−7 of the manuscript). Based on this analysis, at first glance, it appears unlikely that transition metal ions with relatively weak magnetic properties could be effectively separated from solution mixtures using high-gradient magnetic separation (HGMS). Recent experiments showed a detectable enrichment of paramagnetic metal ions in a closed cuvette under LGMS, driven by evaporation,[39−41] or in inertial microfluidic flows under magnetic and/or electric fields.[42] These findings suggest that additional underlying mechanisms may be at play, which warrants further investigation.

The primary goal of this research article is to investigate the transport and separation of transition metal ions under high-gradient magnetic fields and to assess the feasibility of separating metal ions from mixtures. To explore this approach, we investigate two transition metal ions: paramagnetic $MnCl_2$ and diamagnetic $ZnCl_2$. We will evaluate the time evolution of the concentrations of these two metal ions in solution with each individual metal ion and solutions that contain a binary mixture of these metal ions. We also present a simple model to predict the evolution of ion concentration within the separation domain, providing insight into the key forces and the underlying physics that govern the separation of the metal ions in high gradient magnetic fields.

2. MATERIALS AND METHODS

The solutions used in the experiments consist of transition metal ions, specifically manganese(II) chloride ($MnCl_2$) and zinc(II) chloride ($ZnCl_2$), obtained from MilliporeSigma and used as received. The solutions were prepared over a broad range of concentrations from 1 to 100 mM in Millipore water. Two types of aqueous solutions are made: solutions containing single metal ions and solutions containing a binary mixture of these metal ions.

As shown in Figure 1, the flow chamber consists of several parts. The separation process is conducted under the influence of a 1 T electromagnet, which provided a uniform and controlled magnetic field during the experiments. The separation chamber is a single-column fabricated from borosilicate glass with a diameter and length of 1 and 10 cm, respectively. The chamber is filled with a 434-grade steel wool mesh wire with a diameter of 40 μm. The packing density of the mesh wool is measured to be 0.1, which gives the porosity

https://doi.org/10.1021/acs.jpca.4c08312
J. Phys. Chem. A 2025, 129, 3401−3410

of 0.9. Using the Carman-Kozeny relation, the permeability of the mesh wool can be estimated as $6.480 \times 10^{-10} m^2$.[43,44] A peristaltic pump is used to generate a continuous flow velocity of approximately 3.3 mm/s and to circulate the metal-ion solution through a closed-loop system. A small volume of solution (1 mL) is extracted from the solution reservoir (as shown in Figure 1) at 1 h intervals for concentration analysis. To measure the concentration of the metal ions during experiments (at each one-hour interval), the light absorbance of the metal ions in the presence of a coloring agent (Xylenone Orange) is measured via a UV−vis spectrophotometer (3500 Agilent Technologies). Additionally, inductively coupled plasma optical emission spectroscopy (ICP-OES) is used for high-precision ion concentration analysis, particularly in experiments involving binary mixtures of metal ions. The magnetization properties of the materials used in this study were measured by a 16 T quantum design property measurement system (PPMS) superconducting magnet with a vibrating-sample magnetometer option.

3. MODELING MAGNETOPHORETIC SEPARATION

To develop an in-depth understanding of magnetic separation under high gradients, we first analyze the key forces at play in this process. In principle, the ions that move through the HGMS may experience a range of forces, including magnetic force, gravity, diffusion, viscous force, and inertia. Inertia can be assessed using the Reynolds number, which is defined as $\mathrm{Re} = \frac{\rho \mid \mathbf{U}_0 \mid d}{\eta}$, where ρ, $|\mathbf{U}_0|$, d, and η are solution density, average fluid velocity imposed by the pump, wire diameter, and the solution viscosity, respectively. The Reynolds number in the experiments reported in this paper is very low ($\mathrm{Re} \ll 1$). Therefore, inertia is negligible. When dissolved in water, metal ions become hydrated by surrounding water molecules, forming a hydration shell. For single hydrated ions, the effective radius of this hypothetical hydration sphere is approximately $\approx$ 3.5 Å.[45,46] However, the hydration sphere may extend to include a partial second hydration shell, potentially incorporating chloride anions. In this case, the effective radius could increase to approximately $R_s \approx 6$ Å. This hydration shell radius is comparable to the hydrodynamic radius of the metal ion. At this scale, the gravitational forces acting on a hypothetical hydration sphere with $R_s \approx 6$ Å are negligible. On the other hand, under isothermal conditions, the magnetic force that a metal ion with no net charge experiences is related to magnetic energy as[47−49] $\mathbf{F}_m = -\nabla E_{mag}$. Magnetic energy is expressed as $E_{mag} = -\mu_0 V_s \mathbf{M_s H}/2$, where μ_0 is the permeability of free space $\left(4\pi \times 10^{-7} \frac{N}{A^2}\right)$, V_s is the volume of the metal ion, $\mathbf{M_s}$ is the magnetization of the metal ion, and $\mathbf{H}$ is the magnetic field strength created around the ion by the presence of the wire. Therefore, the magnetic force can be expressed as

$$\mathbf{F}_m = \mu_0 V_s (\mathbf{M_s}\cdot\nabla)\mathbf{H} + \frac{\mu_0 V_s \mathbf{M_s H}\cdot\nabla c}{2c} \tag{1}$$

The first term on the right-hand side of eq 1 represents the magnetic force due to field gradients ($F_{\nabla \mathbf{B}}$), while the second term accounts for the contribution from concentration gradients ($F_{\nabla c}$). Our calculations show that $F_{\nabla c}$ is significantly smaller than $F_{\nabla \mathbf{B}}$ in the experiments of this study (see the right panel of Figure A(1) in the Supporting Information and the related discussion). Therefore, throughout the rest of this manuscript, we focus exclusively on the magnetic force arising from field gradients. The magnetic field around the wire depends on the magnetization of the wire $\boldsymbol{M}_w$ and the relative distance from the surface of the wire. In addition to the magnetic force, the metal ion may experience thermal diffusion as a result of Brownian motion. This force could be approximated as $\mathbf{F}_T \approx k_B T/R_s$, where k_B and T are the Boltzmann constant and the absolute temperature, respectively. Finally, in a flowing system, ions will experience a hydrodynamic force that in the absence of inertia could be estimated as $\mathbf{F}_v \approx 6\pi\eta \mathbf{U}_0 R$.

In a multicollector magnetic filter, such as a steel wool separation matrix used in this study and for a paramagnetic ion, the magnetic force is attractive toward the wire, whereas the diffusive and viscous forces are competing against this attractive force. To assess the relative importance of these forces, we can construct two dimensionless numbers. First, the ratio of the magnetic force to thermal diffusion is expressed as a magnetic Peclet number:

$$\mathrm{Pe}_m = \frac{\mathbf{F_m}}{\mathbf{F_T}} = \frac{\mu_0 V_s (\mathbf{M_s}\cdot\nabla)\mathbf{H}}{k_B T/R_s} \tag{2}$$

Note that the magnetic Peclet number varies as a function of the distance from the wire surface. In the vicinity of the wire, where the magnetic field gradient is at its peak, the magnetic Peclet number also reaches its maximum. Previous studies have calculated the maximum magnetic field around a magnetic wire,[30,31,50] which can be used to construct the maximum magnetic Peclet number as

$$\mathrm{Pe}_m|_{max} = \frac{4\pi\mu_o M_{wire} M_s R_s^3}{3k_B T} \tag{3}$$

Here, M_{wire} is the magnetization of the wire. Second, the relative importance of the magnetic force and the viscous forces in the vicinity of the wire can be estimated as a Mason number defined below:

$$\mathrm{Ma}_m|_{max} = \frac{\mathbf{F_m}}{\mathbf{F_v}}|_{max} = \frac{2\mu_o M_{wire} M_s R_s}{9\eta|\mathbf{U}_0|} \tag{4}$$

Depending on the relative importance of these forces, diffusion or flow could be the rate-limiting factor in magnetically separating and capturing the metal ions.

While the above analysis is crucial, it does not enable us to evaluate the temporal variation of the ion concentration within the column. To address this, we will need to apply a mass conservation approach, as outlined below. Because inertia is not important in this work, the HGMS model developed by Watson[32] can not be applied to the experiments. As paramagnetic metal ions move from the top of the column to the bottom and exit the column, a portion of the metal ions is captured by the wires. To evaluate the capture rate of these species in this system, one could write the mass conservation on the species as follows:

$$\frac{\partial n}{\partial t} = -\nabla\cdot(D\nabla n) + \nabla\cdot(n\mathbf{v}) \tag{5}$$

Here n, D, and $\mathbf{v}$ are the number density of species, diffusion coefficient, and fluid velocity. Under steady state conditions, and constant imposed fluid velocity, the mass balance along the separation column height can be written as

https://doi.org/10.1021/acs.jpca.4c08312
J. Phys. Chem. A 2025, 129, 3401−3410

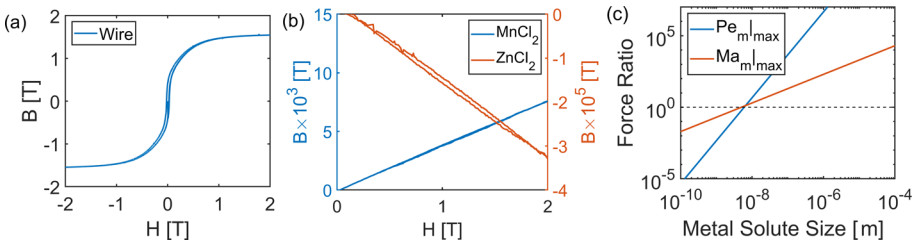

Figure 2. Magnetization curves measured for (a) wire mesh, (b) $MnCl_2$ and $ZnCl_2$ ions. (c) Calculated ratio of forces noted in eqs 3 and 4 as a function of paramagnetic $MnCl_2$ ion size for the experimental conditions used in this study and a magnetic field of 1 T. Below a critical size of $R_c \approx$ 8 nm, the separation process of the metal ions is diffusion limited (diffusion is the rate limiting factor). Beyond this critical size, the separation is limited by viscous forces.

$$\frac{\partial n}{\partial x} = \alpha n \tag{6}$$

Previous studies showed that $\alpha = -f/L$,[30,31,50] where f and L are the fractional capture of species in the column and the length of the column, respectively. The fractional capture of species f is given by the expression below:[30,31]

$$f = \frac{A_c - b}{\phi_i - b} \tag{7}$$

Here $A_c = A(1 - \phi_i)/2\pi$ and ϕ_i, b are the capture area of species around the wire, the initial void fraction of the column before any magnetic buildup occurs, and the magnetic buildup of species in the column, respectively. The magnetic buildup is defined as $b = \phi - \phi_i$, where ϕ is the void fraction in the column. As species move through the column, they accumulate, and the rate of this buildup, impacting the capture efficiency of species by the wire, has been calculated to be[30,31,50]

$$\frac{\partial b}{\partial t} = -\frac{nf}{n_s L}|\mathbf{U_o}| \tag{8}$$

Here, n_s is the number density of species that are captured on the wire. In what follows, we adopt the above model to predict the variation of the ion concentration in our experiments. Note that we calculate the concentration of effluent after each filtration pass by simultaneously solving eqs 5−8. We will then use the existing buildup in the column to assess the variation of the ion concentration for subsequent filtration passes. The details of the equations and computational results for the capture rate under diffusion and flow conditions are discussed in detail in the Supporting Information.

4. RESULTS AND DISCUSSION

4.1. Force Balance Analysis. Prior to discussing the experimental results, we began our analysis by evaluating the dimensionless numbers. To evaluate the dimensionless parameters, we will need the magnetization of the wire and the metal ions. Figure 2a, b presents the magnetization curves of stainless steel mesh wool as well as those of paramagnetic and diamagnetic samples. While the magnetization of the wire saturates for applied magnetic fields above 1 T, the metal ions do not reach saturation within this range of magnetic fields. Using the experimentally determined magnetization of the wire and those of $MnCl_2$, we have calculated the ratio of these two forces as a function of ion size for an applied magnetic field of 1 T, as shown in Figure 2(c). Our calculations indicate that below a critical ion size of approximately 8 nm, diffusive forces dominate, while beyond this threshold, magnetic separation is limited by viscous forces. This simple dimensionless analysis suggests that the ion size must exceed this critical threshold of 8 nm for any meaningful separation of the paramagnetic metal salt from its solution. Notably, this size is significantly larger than the hydration radius of individual metal ions. As noted before, the typical hydration radius for $MnCl_2$ complexes in water is approximately 6 Å.[45,46] Under this condition, both $Pe_m|_{max}$ and $Ma_m|_{max}$ are much smaller than unity, suggesting that no magnetically assisted capture should occur for paramagnetic metal ions. In addition, the magnetic force for diamagnetic $ZnCl_2$ is always negative, indicating that these ions are repelled by the mesh wire. As a result of this force balance, it would be expected that neither paramagnetic nor diamagnetic ions would be captured by the mesh wool. Surprisingly, our experiments demonstrate that magnetic capture can occur for paramagnetic metal ions under certain conditions. In the following sections, we will delve into the experimental results and present a comprehensive analysis of our findings, highlighting the mechanisms behind this unexpected phenomenon.

4.2. Magnetophoretic Separation of Individual Metal Ions from Solution. We began experiments by flowing solutions containing single metal ions in deionized water through the column. To ensure that there were no complications arising from interactions between the stainless-steel mesh wool and the aqueous solutions, we conducted control experiments in parallel, where the magnetic field was kept off. Figure 3a shows the absorbance intensity for these metal ion solutions as a function of concentration. Within this concentration range, the absorbance intensity increases linearly with the concentration of the ion, indicating that the Beer−Lambert law is applicable.[51] This plot serves as a calibration curve to determine the concentration of the metal ions extracted from the column.

Figure 3b illustrates the temporal evolution of the normalized concentrations of paramagnetic $MnCl_2$ for different initial concentrations. The paramagnetic metal ions are captured by the mesh wool, with the capture rate increasing over time. Furthermore, as the initial concentration of $MnCl_2$ increases, the amount of captured metal ions increases (or the normalized concentration of metal ions in the running solution decreases). It is important to note that control experiments, where the magnetic field was turned off, showed no significant change in the concentration of the paramagnetic $MnCl_2$ ions over time. This indicates that the observed capture is directly related to the presence of the magnetic field. Figure 3(c) shows the temporal variation of the normalized concentration for diamagnetic $ZnCl_2$ ions across a wide range of initial concentrations. The concentration remains unchanged, even

https://doi.org/10.1021/acs.jpca.4c08312
J. Phys. Chem. A 2025, 129, 3401−3410

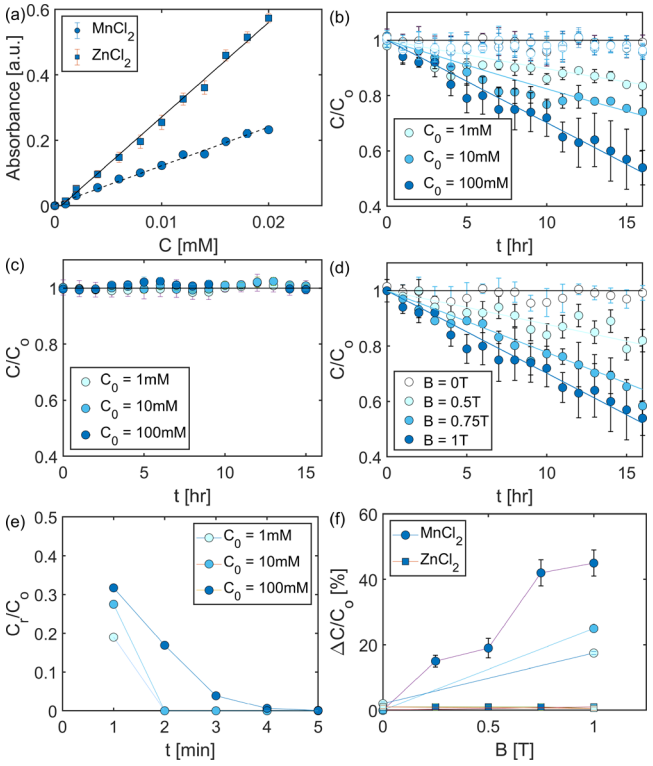

Figure 3. (a) Calibration curves measured for both metal ions. The slopes of these linear lines that are best fitted to the experimental data are 11.82 and 28.88 for $MnCl_2$ and $ZnCl_2$, respectively. (b) Normalized concentration of captured $MnCl_2$ metal ions as a function of time for a broad range of initial concentrations. The filled and open symbols correspond to magnetic field of 1 and 0 T, respectively. (c) Normalized concentration of $ZnCl_2$ metal ions as a function of time for a broad range of initial concentrations at a magnetic field of 1 T. (d) The normalized captured concentration of $MnCl_2$ as a function of time for various imposed magnetic fields and C_0 = 100 mM. (e) Normalized recovered $MnCl_2$ concentration as a function of flushed time for various initial concentrations after the field was turned off from 1 T. (f) Overall change in concentration of the metal ions as a function of applied magnetic field after 16 h of experiments. The light to dark colors indicate C_0 = 1, 10, and 100 mM, respectively.

after 16 h. Unlike paramagnetic ions, the diamagnetic $ZnCl_2$ ions do not interact with the magnetic mesh wool and, therefore, are not captured by the stainless-steel mesh. Diamagnetic $ZnCl_2$ ions are expected to experience a repulsive force from the magnetic mesh since their magnetic susceptibility is less than that of deionized water. Such an effect is not expected to impact the output of $ZnCl_2$ ions as evidenced by Figure 3(c). In addition, the effect of varying the external magnetic field strengths on the capture rate of paramagnetic $MnCl_2$ was studied. Figure 3(d) illustrates the normalized concentration of $MnCl_2$ as a function of time for different magnetic field intensities. As the imposed magnetic field strength increases, the overall rate of ion capture rises correspondingly. These results support our hypothesis that the separation process is induced by the influence of an external magnetic field.

To further confirm this hypothesis, we turned off the magnetic field following the experiments and subsequently flushed the chamber with purified water. The concentration of the metal ion in the flushed fluid was measured at 1 min time intervals. Figure 3e presents the normalized concentration of recovered metal ions as a function of time for three distinct initial concentrations, following experiments conducted at a magnetic field strength of B = 1 T. The data demonstrate that paramagnetic ions can be recovered from the chamber upon deactivation of the magnetic field, thereby reinforcing our hypothesis that the separation process is driven by the external magnetic field. Furthermore, the results underscore the reversible nature of the magnetic capture in these systems. Finally, Figure 3f summarizes the capture rate of the two metal ions after 16 h of magnetic field exposure, plotted against the applied magnetic field across the range of initial concentrations tested in this study. The results clearly indicate that magnetic separation is enhanced with increasing magnetic field strength, with higher initial concentrations yielding greater separation efficiency for the paramagnetic $MnCl_2$ ions. In contrast, the diamagnetic $ZnCl_2$ ions show no interaction with the magnetic field, regardless of its strength or the initial ion concentration, and thus, their concentration remains unchanged throughout the experiments.

As indicated by force balance analysis, magnetically assisted capture was not anticipated for paramagnetic metal ions. This raises the question of what might have contributed to this discrepancy in our experimental results. The direct measurement of the forces acting on metal ions presents significant challenges. However, we can gain further insight into this issue by examining the theoretically predicted temporal evolution of the metal ion concentration and comparing it with our experimentally measured values. This comparison could help elucidate the underlying factors influencing the observed magnetic capture. In our first attempt to calculate the concentration variation in the domain, we solved eqs 5−8 by using the typical hydration radii of the metal ions in solution as a reference (e.g., approximately 6 Å for $MnCl_2$ and $ZnCl_2$[45,46]). Under these conditions, the paramagnetic $MnCl_2$ shows no interaction with the magnetic field, as indicated by the normalized concentration remaining around unity, suggesting no magnetic capture (see the horizontal line in Figure 3(b)). This result aligns with the previously presented force balance analysis.

To find the best match between experiments and the model, we increased the R_s values beyond the hydration radius of the metal ion to obtain the best fit with the experimental data. The continuous lines in Figure 3(b) represent the best fit of the model to the experimental data points. Furthermore, the model was fitted to the experimental results obtained at different magnetic field strengths, as shown in Figure 3d. Table 1 provides a summary of the ion radii that yielded the best fit with the experimental data. Several observations can be made here. First, it is noteworthy that the effective ion size that correlates best with the experimental results is substantially

Table 1. Model Parameters Used To Find the Best Match with Experimental Data Measured in the Separation Chamber

solution	ion	c_0 [mM]	**B** [T]	R_s [nm]
single	$MnCl_2$	1	1	15.4
		10	1	13.8
		100	1	11.8
		100	0.75	13.2
		100	0.5	15.8
		100	0.25	22.1

https://doi.org/10.1021/acs.jpca.4c08312
J. Phys. Chem. A 2025, 129, 3401−3410

larger, by nearly two orders of magnitude, than the hydration radius of the individual metal ions. This observation suggests that the paramagnetic metal ions may have aggregated into clusters under the influence of the magnetic field, leading to their enhanced capture rates in the experiments. Previous studies have demonstrated that transition metal ions in porous media experience a pronounced magnetophoresis effect, much stronger than predicted by a force balance in individual metal ions.[52−54] Researchers have hypothesized that this discrepancy may be due to the formation of ion clusters under the influence of a nonuniform magnetic field. This hypothesis aligns with the findings from our experimental and modeling efforts discussed above. The concept of magnetic field-induced cluster formation is well-established and has been extensively studied in colloidal systems and suspensions of superparamagnetic nanoparticles through both experimental investigations and theoretical modeling.[55−60] Prior research has explored the fundamental mechanisms governing cluster formation, including the interplay between particles' dipole−dipole interactions, electrostatic repulsion, and van der Waals forces under uniform applied magnetic fields.[55−60] Under a uniform magnetic field, two fundamental conditions must be satisfied for field-induced particle clustering to occur. First, magnetic forces, primarily governed by dipole−dipole interactions, must be strong enough to overcome random thermal motion. Second, the particle concentration must be sufficiently high to ensure that the rate of aggregation surpasses the rate of dissociation. The strength of these magnetic interactions can be effectively characterized by the magnetic coupling parameter, Γ, which serves as a key determinant of the system's clustering behavior. For paramagnetic particles, Γ is defined as[59]

$$\Gamma = \frac{\pi R_3^{\mathrm{p}} \Delta\chi^2 \mathbf{B}^2}{9\mu_0 k_{\mathrm{B}} T} \tag{9}$$

Here, $\Delta\chi$ is the difference between the magnetic susceptibility of the metal ion and the solvent, R_{p} is the particle radius, and $\mathbf{B}$ is the magnetic flux density. The latter condition for field-induced particle cluster formation is quantified through the parameter N^*, which is given by

$$N^* = \sqrt{\frac{c_0}{\rho_{\mathrm{p}}} \exp(\Gamma - 1)} \tag{10}$$

Here ρ_{p} is the density of the metal ion in the solution. Field-induced aggregation is expected only when $\Gamma > 1$ and $N^* > 1$. Figure 4 illustrates the variation of N^* and Γ as a function of magnetic field strength and R_{p} for paramagnetic metal ions of $MnCl_2$. For an initial concentration of c_0 = 100 mM, the analysis predicts field-induced aggregation only for $R_{\mathrm{p}} > 220$ nm and $\mathbf{B} \geq 1$ T. According to this analysis, the effective particle (or cluster) size that is required for the formation of field-induced cluster formation is much larger than the values predicted by our 1D numerical simulations of the HGMS (see data in Table 1).

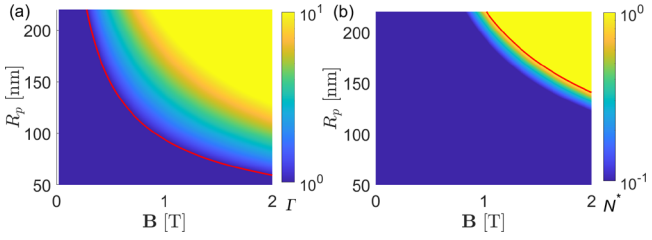

Figure 4. 2D heat map of dimensionless parameters Γ (a), and N^* (b). The red curve shows Γ = 1 and N^* = 1 for each subplot.

This discrepancy is not unexpected. It is crucial to recognize that the above analysis, based on Γ and N^*, applies strictly to uniform magnetic fields and does not account for the influence of strong magnetic field gradients. In the presence of field gradients, a magnetophoretic force may arise, effectively driving metal ions toward the wire and facilitating their mutual attraction. In our study, the magnetic field gradients around individual wires are exceptionally high. Analytical solution to the magnetic field around a ferromagnetic wire[61] indicates that the magnetic field gradients near the wire surface can reach $(\mathbf{B}\cdot\nabla)\mathbf{B}|_{\max} \approx 10^5$ T^2/m and above (see left panel of Figure A(1) in the Supporting Information.), an exceptionally strong gradient capable of inducing metal ion migration toward the wire and potentially facilitating cluster formation. As demonstrated in our analysis of Figure 2, the magnetophoretic force can surpass thermal diffusion (i.e., $\mathrm{Pe_m} > 1$) for $R_{\mathrm{s}} \approx 6$ nm, and the hydrodynamic force (i.e., $\mathrm{Ma_m} > 1$) for $R_{\mathrm{s}} \approx 5$ nm, highlighting the significant role of magnetic field gradients in governing metal ion dynamics. Hence, future investigations into field-induced cluster formation should refine the interaction potential between particles to incorporate the effects of magnetophoretic forces under nonuniform magnetic fields. This refinement will enable a more comprehensive understanding of cluster formation mechanisms, particularly in the presence of strong magnetic field gradients.[55]

Additionally, the data in Table 1 indicate that at a fixed external magnetic field strength ($\mathbf{B}$ = 1 T), an increase in the initial metal ion concentration results in a slight decrease in the minimum cluster size (R_{s}) required to align simulations with experiments. Furthermore, as the magnetic field strength increases, the R_{s} decreases even further. These findings are somewhat unexpected, as one would anticipate, based on the analysis presented in Figure 4, that higher magnetic field strengths and initial concentrations would promote the formation of larger clusters (or lead to larger effective cluster sizes). It is important to highlight that in the discussion above, we have not yet considered the potential formation of secondary flows in the HGMS near wire surfaces. In regions where magnetic forces are strong, such as near the wire surface, the transport of metal ions may impart momentum to the surrounding fluid, potentially leading to the development of secondary flows. It is well established that secondary flow formation can significantly enhance the magnetophoretic transport of superparamagnetic nanoparticles.[62,63] Moreover, these secondary flows may not only influence but also compete with field-induced particle cluster formation, potentially altering the overall separation dynamics. The strength of such secondary flows can be characterized by the dimensionless magnetic Grashof number $\mathrm{Gr_m}$. If $\mathrm{Gr_m} < 1$, secondary flows are weak and have minimal impact on separation. Conversely, when $\mathrm{Gr_m} > 1$, secondary flows become significant, influencing the separation dynamics. The magnetic Grashof number $\mathrm{Gr_m}$ can be defined as[63]

$$\mathrm{Gr_m} = \frac{\rho_{\mathrm{p}} \Delta\chi c_0 L^3}{\mathcal{M}_{\mathrm{i}}(1 + \chi V, f)\mu_0 \eta^2} |(\mathbf{B}\cdot\nabla)\mathbf{B}|_{\max} \tag{11}$$

Here, $\mathcal{M}_i$, and χ_{V_f} are the molecular weight of the species in the solution, and the volumetric magnetic susceptibility of the

https://doi.org/10.1021/acs.jpca.4c08312
J. Phys. Chem. A 2025, 129, 3401−3410

fluid, respectively. Figure 5 illustrates the magnetic Grashof number, Gr_m, computed as a function of the initial

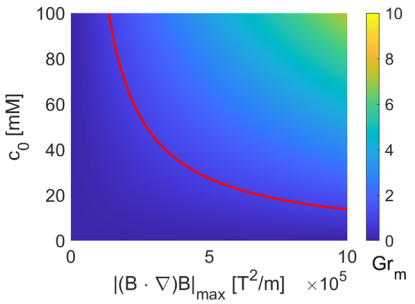

Figure 5. Variation of the magnetic Grashof number with $(\mathbf{B}\cdot\nabla)\mathbf{B}|_{max}$ and initial concentration of paramagnetic metal ions of $MnCl_2$ in the solution. The red line marks $Gr_m = 1$.

concentration and magnetic field gradients for the HGMS experimental parameters. There exist regions where $Gr_m > 1$, suggesting that secondary flows play a significant role in the separation process in this study. We hypothesize that metal ion separation in HGMS is governed by the interplay of two dominant mechanisms: (i) field-induced cluster formation and (ii) secondary flows. At low initial concentrations (e.g., $c_0 = 1$ mM) where $Gr_m < 1$, separation is primarily driven by field-induced cluster formation. However, as the initial concentration increases, Gr_m may transition beyond unity, for which secondary flows emerge as a significant factor enhancing separation. In this regime, separation efficiency likely benefits from the synergistic interaction of both mechanisms, potentially altering clustering dynamics. Thus, larger clusters are not necessarily required at higher concentrations; instead, secondary flows facilitate separation with smaller cluster sizes. In another example, at a fixed metal ion concentration (e.g., c_0 = 100 mM), increasing the applied magnetic field strength (or $|(\mathbf{B}\cdot\nabla)\mathbf{B}|_{max}$) further amplifies secondary flow effects, reducing the need for large clusters to achieve efficient separation. The observed trends in R_s values (Table 1) support this hypothesis.

4.3. Magnetophoretic Separation of Metal Ions from Binary Mixtures. In end-of-life LIBs, electronics, and many practical applications, metal ions with different magnetic properties often exist in mixtures, making it crucial to develop methods that enable their effective separation from each other within the mixture. Achieving selective separation of two ions based on magnetic properties could be particularly beneficial in such contexts. Therefore, in this section, we examined the separation of paramagnetic $MnCl_2$ from diamagnetic $ZnCl_2$ in a binary mixture of these ions.

Figure 6a,b shows the normalized concentrations of $MnCl_2$ and $ZnCl_2$ in an equimolar mixture (100 mM) under varying magnetic fields. At a higher magnetic field strength of 1 T, $MnCl_2$ is effectively captured by the mesh, while the diamagnetic ions remain largely unaffected by the presence of the magnetic field or the paramagnetic metal ions. As a result, the diamagnetic $ZnCl_2$ ions exit the column at their initial concentration. Consistent with the single-component solution experiments, increasing the magnetic field and the initial concentration of metal ions increases the capture rate of paramagnetic $MnCl_2$, as shown in Figure 6(c).

Perhaps equally important is the observation that the capture rate of the paramagnetic metal ion in a binary mixture is reduced compared to that measured in solutions containing individual paramagnetic or diamagnetic ions (cf. Figures 6(c) and 3(f)). To model the separation process in the binary mixture, we assume that the effective magnetization of the mixture is a weighted average of the magnetization of the individual metal ions. This can be expressed as $M_s = \sum x_i M_i$, where x_i represents the fraction of each metal ion in the mixture, and M_i denotes the magnetization of each ion. For this case, $x_i = 0.5$ for each component. Using this effective magnetization for the binary mixture, we fitted the above model to the experimental data for mixtures under different magnetic field strengths. The resulting predictions are shown as continuous curves in Figure 6a, b). The critical radii values that produce the best match with mixture experiments turn out to be larger than those noted in Table 1 ($R_s \approx 20.3$ and 15 nm for $B = 0.5$ T and $B = 1$ T, respectively). These results underscore the impact of magnetic field strength on ion capture and highlight the complexity of separating metal ions in mixtures.

5. CONCLUSIONS

In summary, we report the first experimental demonstration of separating paramagnetic and diamagnetic metal ions, specifically $MnCl_2$ and $ZnCl_2$, from a solution mixture by using high-gradient magnetic fields generated by a stainless steel mesh. This study highlights the potential for the use of magnetic fields to selectively capture metal ions on the basis of their magnetic properties. Our experiments were conducted on solutions containing either individual metal ions or binary aqueous mixtures. For solutions with single metal ions, the paramagnetic $MnCl_2$ is effectively attracted to the magnetic mesh wool, whereas diamagnetic $ZnCl_2$ remains unaffected by

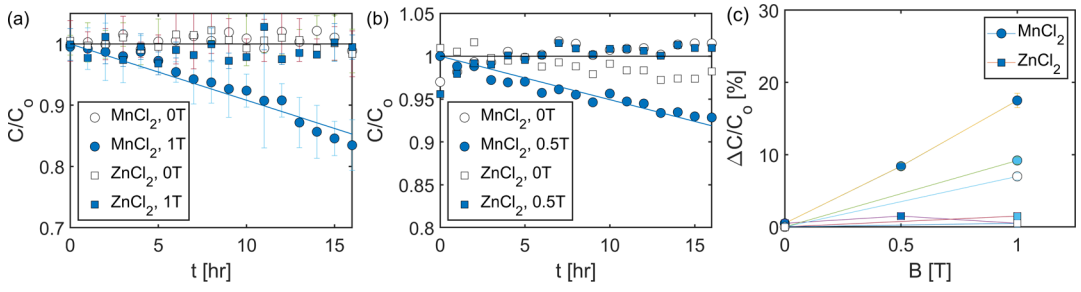

Figure 6. Normalized concentration of the $MnCl_2$ and $ZnCl_2$ metal ions as a function of time for binary mixtures containing both paramagnetic and diamagnetic ions at two magnetic field strengths: (a) $B = 1$ T and (b) $B = 0.5$ T. The overall concentration change (percentile) as a function of the applied magnetic field for both paramagnetic and diamagnetic metal ions is depicted for binary mixtures. In (c), the concentration of metal ions changes from 1, 10, and 100 mM for symbols from white to dark blue.

https://doi.org/10.1021/acs.jpca.4c08312
J. Phys. Chem. A 2025, 129, 3401−3410

the magnetic field gradients. We observed that increasing the initial concentration of the paramagnetic metal ion and the external magnetic field strength enhances the rate of magnetic capture.

In binary mixtures, paramagnetic metal ions are preferentially captured by the magnetic mesh wool, while diamagnetic ions are not retained. Additionally, the capture rate for paramagnetic metal ions increases as both the magnetic field strength and initial ion concentration are raised. The capture rate of paramagnetic ions in binary mixtures is lower than that observed in solutions containing only single metal ions. We hypothesize that the presence of the diamagnetic ion in the mixture reduces the overall magnetization of the paramagnetic ion clusters because of the presence of Zn ions in the Mn ion clusters. This reduction in magnetization leads to a decreased attraction to the magnetic mesh wires, resulting in a lower capture rate for the paramagnetic ion. The inferred sizes of clusters are larger in binary mixtures of metal ions than in the individual ions of the same elements, which implies that the diamagnetic ion enters the ionic clusters of the paramagnetic ion, lowering the overall separation efficiency of the HGMS.

Furthermore, we modeled the magnetic separation of these metal ions using a multiphysics framework, which incorporates magnetic, viscous, and diffusive forces. Our modeling indicates that to achieve the observed levels of magnetic capture (10−50% depending on the conditions), the paramagnetic metal ions must aggregate into clusters significantly larger than their individual units, approximately in the order of $\approx O(10)$ nanometer under the influence of the magnetic field. Our analysis shows that in addition to field-induced cluster formation, secondary flows may be present near the wire surface and facilitate the separation of metal ions. Future studies should directly quantify the relative contributions of secondary flows and field-induced cluster formation in the magnetophoretic transport of metal ions near a wire surface. We anticipate that these results will offer valuable insight into the recycling and recovery of critical metals from electronic devices. Additionally, they may open avenues for innovative strategies in various applications, such as the transport of ferromagnetic nanoparticles for drug delivery, protein separation, and water purification.

■ ASSOCIATED CONTENT

Supporting Information

The Supporting Information is available free of charge at https://pubs.acs.org/doi/10.1021/acs.jpca.4c08312.

Additional information on details of the magnetic field and modeling HGMS (PDF)

■ AUTHOR INFORMATION

Corresponding Author

Hadi Mohammadigoushki − *Department of Chemical and Biomedical Engineering, FAMU-FSU College of Engineering, Tallahassee, Florida 32310, United States; Center for Rare Earths, Critical Minerals, and Industrial Byproducts, National High Magnetic Field Laboratory, Tallahassee, Florida 32310, United States;* orcid.org/0000-0002-7240-2215; Email: hadi.moham@eng.famu.fsu.edu

Authors

Prateek Benhal − *Department of Chemical and Biomedical Engineering, FAMU-FSU College of Engineering, Tallahassee, Florida 32310, United States; Center for Rare Earths, Critical Minerals, and Industrial Byproducts, National High Magnetic Field Laboratory, Tallahassee, Florida 32310, United States*

Muhammad Garba − *Department of Chemical and Biomedical Engineering, FAMU-FSU College of Engineering, Tallahassee, Florida 32310, United States; Center for Rare Earths, Critical Minerals, and Industrial Byproducts, National High Magnetic Field Laboratory, Tallahassee, Florida 32310, United States;* orcid.org/0000-0003-4633-8675

Jamel Ali − *Department of Chemical and Biomedical Engineering, FAMU-FSU College of Engineering, Tallahassee, Florida 32310, United States; Center for Rare Earths, Critical Minerals, and Industrial Byproducts, National High Magnetic Field Laboratory, Tallahassee, Florida 32310, United States*

Theo Siegrist − *Department of Chemical and Biomedical Engineering, FAMU-FSU College of Engineering, Tallahassee, Florida 32310, United States; Center for Rare Earths, Critical Minerals, and Industrial Byproducts, National High Magnetic Field Laboratory, Tallahassee, Florida 32310, United States;* orcid.org/0000-0001-5368-1442

Munir Humayun − *Center for Rare Earths, Critical Minerals, and Industrial Byproducts, National High Magnetic Field Laboratory, Tallahassee, Florida 32310, United States; Department of Earth, Ocean and Atmospheric Science, Florida State University, Tallahassee, Florida 32306, United States*

Complete contact information is available at: https://pubs.acs.org/10.1021/acs.jpca.4c08312

Notes

The authors declare the following competing financial interest(s): The authors have an IP on this research area. The authors have patent disclosure on this subject research area with US Application No. 63/719,917.

■ ACKNOWLEDGMENTS

A portion of this work was performed at the National High Magnetic Field Laboratory, which is supported by the National Science Foundation Cooperative Agreement No. DMR-1644779 and the state of Florida. Additionally, HM gratefully acknowledges the support from the National Science Foundation through award CET 2343151. This work was supported by the Center for Rare Earths, Critical Minerals, and Industrial Byproducts, through funding provided by the State of Florida. We greatly appreciate fruitful discussions with Peter Rassolov of the National High Magnetic Field Laboratory.

■ REFERENCES

(1) Gunther, C. G.; *Electro-Magnetic Ore Separation*; Hill Publishing Company: New York, 1909.

(2) Dames, P.; Gleich, B.; Flemmer, A.; Hajek, K.; Seidl, N.; Wiekhorst, F.; Eberbeck, D.; Bittmann, I.; Bergemann, C.; Weyh, T.; et al. Targeted delivery of magnetic aerosol droplets to the lung. *Nat. Nanotechnol.* **2007**, *2* (8), 495−499.

(3) Steiner, U. E.; Ulrich, T. Magnetic field effects in chemical kinetics and related phenomena. *Chem. Rev.* **1989**, *89* (1), 51−147.

(4) Yavuz, C. T.; Mayo, J. T.; Yu, W. W.; Prakash, A.; Falkner, J. C.; Yean, S.; Cong, L.; Shipley, H. J.; Kan, A.; Tomson, M.; et al. Low-field magnetic separation of monodisperse fe3o4 nanocrystals. *Science* **2006**, *314* (5801), 964−967.

(5) Lim, J. K.; Yeap, S. P.; Low, S. C. Challenges associated to magnetic separation of nanomaterials at low field gradient. *Sep. Purif. Technol.* **2014**, *123*, 171−174.
(6) Kemsheadl, J. T.; Ugelstad, J. Magnetic separation techniques: their application to medicine. *Mol. Cell. Biochem.* **1985**, *67*, 11−18.
(7) Ito, A.; Shinkai, M.; Honda, H.; Kobayashi, T. Medical application of functionalized magnetic nanoparticles. *J. Biosci. Bioeng.* **2005**, *100* (1), 1−11.
(8) Işıldar, A.; van Hullebusch, E. D.; Lenz, M.; Du Laing, G.; Marra, A.; Cesaro, A.; Panda, S.; Akcil, A.; Kucuker, M. A.; Kuchta, K. Biotechnological strategies for the recovery of valuable and critical raw materials from waste electrical and electronic equipment (weee)−a review. *J. Hazard. Mater.* **2019**, *362*, 467−481.
(9) Chan, K. H.; Anawati, J.; Malik, M.; Azimi, G. Closed-loop recycling of lithium, cobalt, nickel, and manganese from waste lithium-ion batteries of electric vehicles. *ACS Sustainable Chem. Eng.* **2021**, *9* (12), 4398−4410.
(10) Chan, K. H.; Malik, M.; Azimi, G. Separation of lithium, nickel, manganese, and cobalt from waste lithium-ion batteries using electrodialysis. *Resources, Conservation and Recycling* **2022**, *178*, No. 106076.
(11) He, J.; Huang, M.; Wang, D.; Zhang, Z.; Li, G. Magnetic separation techniques in sample preparation for biological analysis: a review. *J. Pharm. Biomed. Anal.* **2014**, *101*, 84−101.
(12) Mariani, G.; Fabbri, M.; Negrini, F.; Ribani, P. L. High-gradient magnetic separation of pollutant from wastewaters using permanent magnets. *Sep. Purif. Technol.* **2010**, *72* (2), 147−155.
(13) Sierra, C.; Martínez, J.; Menéndez-Aguado, J. M.; Afif, E.; Gallego, J. R. High intensity magnetic separation for the clean-up of a site polluted by lead metallurgy. *J. Hazard. Mater.* **2013**, *248*, 194−201.
(14) Qin, Y.; Yao, Z.; Ruan, J.; Zhenming, X. Motion behavior model and multistage magnetic separation method for the removal of impurities from recycled waste plastics. *ACS Sustainable Chem. Eng.* **2021**, *9* (32), 10920−10928.
(15) Iranmanesh, M.; Hulliger, J. Magnetic separation: its application in mining, waste purification, medicine, biochemistry and chemistry. *Chem. Soc. Rev.* **2017**, *46* (19), 5925−5934.
(16) Sugden, S. Magnetochemistry. *Journal of the Chemical Society (Resumed)* **1943**, 328−333.
(17) Oberteuffer, J. High gradient magnetic separation. *IEEE Trans. Magn.* **1973**, *9* (3), 303−306.
(18) Kolm, H.; Oberteuffer, J.; Kelland, D. High-gradient magnetic separation. *Sci. Am.* **1975**, *233* (5), 46−55.
(19) Katz, D. H.; McCarthy, J. P.Materials for high gradient magnetic separation. *J. Magn. Magn. Mater.* **1984**, *37*, 301-308.
(20) Mori, Y.; Noguchi, K.; Inoue, K. Development of high gradient magnetic separation. *IEEE Trans. Magn.* **1992**, *28* (4), 2344−2346.
(21) Gerber, F. E.Advances in high gradient magnetic separation. *Miner. Eng.* **1995**, *8*, 5, 575-583.
(22) Luborsky, F. E. B. J.; Drummond, B. High gradient magnetic separation: Theory versus experiment. *IEEE Trans. Magn.* **1975**, *11* (6), 1696−1700.
(23) Xue, Z.; Wang, Y.; Zheng, X.; Dongfang, L.; Jing, Z.; Li, X.; Zhicheng, H.; Wang, Y. Role of gravitational force on mechanical entrainment of nonmagnetic particles in high gradient magnetic separation. *Miner. Eng.* **2022**, *186*, No. 107726.
(24) Watson, J. H. P.; Li, Z. Theoretical and single-wire studies of vortex magnetic separation. *Miner. Eng.* **1992**, *5* (10−12), 1147−1165.
(25) Xue, Z.; Wang, Y.; Zheng, X.; Dongfang, L.; Li, X. Particle capture of special cross-section matrices in axial high gradient magnetic separation: A 3d simulation. *Sep. Purif. Technol.* **2020**, *237*, No. 116375.
(26) Chen, L.; Zeng, J.; Guan, C.; Zhang, H.; Yang, R. High gradient magnetic separation in centrifugal field. *Miner. Eng.* **2015**, *78*, 122−127.
(27) Zheng, X.; Wang, Y.; Dongfang, L.; Li, X. Theoretical and experimental study on elliptic matrices in the transversal high gradient magnetic separation. *Miner. Eng.* **2017**, *111*, 68−78.
(28) Zeng, J.; Tong, X.; Yi, F.; Chen, L. Selective capture of magnetic wires to particles in high gradient magnetic separation. *Minerals* **2019**, *9* (9), 509.
(29) Ye, F.; Deng, H.; Guo, Z.; Wei, B.; Ren, X. Separation mechanism and experimental investigation of pulsating high gradient magnetic separation. *Results in Physics* **2023**, *49*, No. 106482.
(30) Ditsch, A.; Lindenmann, S.; Laibinis, P. E.; Wang, D. I. C.; Hatton, A. T. High-gradient magnetic separation of magnetic nanoclusters. *Ind. Eng. Chem. Res.* **2005**, *44* (17), 6824−6836.
(31) Moeser, G. D.; Roach, K. A.; Green, W. H.; Alan Hatton, T.; Laibinis, P. E. High-gradient magnetic separation of coated magnetic nanoparticles. *AIChE J.* **2004**, *50* (11), 2835−2848.
(32) Watson, J.-H. Magnetic filtration. *J. Appl. Phys.* **1973**, *44* (9), 4209−4213.
(33) Watson, J. Theory of capture of particles in magnetic high-intensity filters. *IEEE Trans. Magn.* **1975**, *11* (5), 1597−1599.
(34) Svoboda, J. A realistic description of the process of high-gradient magnetic separation. *Miner. Eng.* **2001**, *14* (11), 1493−1503.
(35) Sandulyak, A. V.; *Magnetic Filtration of Liquids and Gases*; Ximiya: Moscow, pp 40−80, 1988.
(36) Abbasov, T.; Koksal, M.; Herdem, S. Theory of high-gradient magnetic filter performance. *IEEE Trans. Magn.* **1999**, *35* (4), 2128−2132.
(37) Abbasov, T.; Altunbas, A. S. Determination of the particle capture radius in magnetic filters with velocity distribution profile in pores. *Sep. Sci. Technol.* **2002**, *37* (9), 2037−2053.
(38) Arajs, S.; Moyer, C. A.; Aidun, R.; Matijevic', E. Magnetic filtration of submicroscopic particles through a packed bed of spheres. *J. Appl. Phys.* **1985**, *57* (8), 4286−4288.
(39) Rodrigues, I. R.; Lukina, L.; Dehaeck, S.; Colinet, P.; Binnemans, K.; Fransaer, J. Magnetomigration of rare-earth ions triggered by concentration gradients. *J. Phys. Chem. Lett.* **2017**, *8* (21), 5301−5305.
(40) Lei, Z.; Fritzsche, B.; Eckert, K. Magnetic separation of rare-earth ions: Transport processes and pattern formation. *Phys. Rev. Fluids* **2021**, *6* (2), L021901.
(41) Yang, X.; Tschulik, K.; Uhlemann, M.; Odenbach, S.; Eckert, K. Enrichment of paramagnetic ions from homogeneous solutions in inhomogeneous magnetic fields. *J. Phys. Chem. Lett.* **2012**, *3* (23), 3559−3564.
(42) Schroeder, B.; Free, M.; Sarswat, P.; Sadler, E.; Burke, J.; Evans, Z. Evaluating field-effect separation on rare earth and critical metals. *Eng.* **2024**, *5* (3), 2016−2032.
(43) Schulz, R.; Ray, N.; Zech, S.; Rupp, A.; Knabner, P. Beyond kozeny−carman: predicting the permeability in porous media. *Transport in Porous Media* **2019**, *130*, 487−512.
(44) Rehman, M.; Hafeez, M. B.; Krawczuk, M. A comprehensive review: Applications of the kozeny−carman model in engineering with permeability dynamics. *Arch. Comput. Methods Eng.* **2024**, 1−13.
(45) Persson, I. Structure and size of complete hydration shells of metal ions and inorganic anions in aqueous solution. *Dalton Trans.* **2024**, *53*, 15517−15538.
(46) Marcus, Y. Ionic radii in aqueous solutions. *Chem. Rev.* **1988**, *88* (8), 1475−1498.
(47) Simon, M. D.; Geim, A. K. Diamagnetic levitation: Flying frogs and floating magnets. *J. Appl. Phys.* **2000**, *87* (9), 6200−6204.
(48) Parker, R. J.; Advances in permanent magnetism. Wiley: New York.
(49) Rassolov, P.; Ali, J.; Siegrist, T.; Humayun, M.; Mohammadigoushki, H. Magnetophoresis of paramagnetic metal ions in porous media. *Soft Matter* **2024**, *20* (11), 2496−2508.
(50) Fletcher, D. Fine particle high gradient magnetic entrapment. *IEEE Trans. Magn.* **1991**, *27* (4), 3655−3677.
(51) Swinehart, D. F. The beer-lambert law. *J. Chem. Educ.* **1962**, *39* (7), 333.

https://doi.org/10.1021/acs.jpca.4c08312
J. Phys. Chem. A 2025, 129, 3401−3410

(52) Fujiwara, M.; Chie, K.; Sawai, J.; Shimizu, D.; Tanimoto, Y. On the movement of paramagnetic ions in an inhomogeneous magnetic field. *J. Phys. Chem. B* **2004**, *108* (11), 3531−3534.
(53) Fujiwara, M.; Mitsuda, K.; Tanimoto, Y. Movement and diffusion of paramagnetic ions in a magnetic field. *J. Phys. Chem. B* **2006**, *110* (28), 13965−13969.
(54) Franczak, A.; Binnemans, K.; Fransaer, J. Magnetomigration of rare-earth ions in inhomogeneous magnetic fields. *Phys. Chem. Chem. Phys.* **2016**, *18* (39), 27342−27350.
(55) Tsouris, C.; Scott, T. C. Flocculation of paramagnetic particles in a magnetic field. *J. Colloid Interface Sci.* **1995**, *171* (2), 319−330.
(56) Faraudo, J.; Andreu, J. S.; Calero, C.; Camacho, J. Predicting the self-assembly of superparamagnetic colloids under magnetic fields. *Adv. Funct. Mater.* **2016**, *26* (22), 3837−3858.
(57) Faraudo, J.; Andreu, J. S.; Camacho, J. Understanding diluted dispersions of superparamagnetic particles under strong magnetic fields: a review of concepts, theory and simulations. *Soft Matter* **2013**, *9* (29), 6654−6664.
(58) Andreu, J. S.; Camacho, J.; Faraudo, J. Aggregation of superparamagnetic colloids in magnetic fields: the quest for the equilibrium state. *Soft Matter* **2011**, *7* (6), 2336−2339.
(59) Jing Liu, E. M.; Lawrence, A. W.; Ivey, M. L.; Flores, G. A.; Javier, K.; Bibette, J.; Richard, J. Field-induced structures in ferrofluid emulsions. *Phys. Rev. Lett.* **1995**, *74* (14), 2828.
(60) De Las Cuevas, G.; Faraudo, J.; Camacho, J. Low-gradient magnetophoresis through field-induced reversible aggregation. *J. Phys. Chem. C* **2008**, *112* (4), 945−950.
(61) Svoboda, J.; *Magnetic techniques for the treatment of materials*. Springer Science & Business Media: Berlin, 2004.
(62) Leong, S. S.; Ahmad, Z.; Lim, J. K. Magnetophoresis of superparamagnetic nanoparticles at low field gradient: hydrodynamic effect. *Soft Matter* **2015**, *11* (35), 6968−6980.
(63) Leong, S. S.; Ahmad, Z.; Low, S. C.; Camacho, J.; Faraudo, J.; Lim, J. K. Unified view of magnetic nanoparticle separation under magnetophoresis. *Langmuir* **2020**, *36* (28), 8033−8055.

https://doi.org/10.1021/acs.jpca.4c08312
J. Phys. Chem. A 2025, 129, 3401−3410